Journal of Drug Delivery Science and Technology 95 (2024) 105541

Contents lists available at ScienceDirect

Journal of Drug Delivery Science and Technology

journal homepage: www.elsevier.com/locate/jddst

Gas foamed scaffolds as smart 3D structures in skin tissue engineering

Eleonora Bianchi [a,1], Marco Ruggeri [a,1], Barbara Vigani [a], Carlotta Totaro Fila [b], Antonia Icaro Cornaglia [c], Cinzia Boselli [a], César Viseras [d], Silvia Rossi [a], Giuseppina Sandri [a,*]

[a] Department of Drug Sciences, University of Pavia, Viale Taramelli 12, 27100, Pavia, Italy
[b] Alia Insect Farm, Via Olmetto, 20123, Milan, Italy
[c] Department of Public Health, Experimental and Forensic Medicine, University of Pavia, via Forlanini 2, 27100, Pavia, Italy
[d] Department of Pharmacy and Pharmaceutical Technology, Faculty of Pharmacy, University of Granada, Campus of Cartuja s/n, Granada, 18071, Spain

ARTICLE INFO

Keywords:
Electrospinning
Gas foaming
Hydroxyapatite
Pullulan
Antioxidant and anti-inflammatory
Tissue regeneration

ABSTRACT

Globally, wound care is a major problem that poses big issues for national healthcare systems. Consequently, the development of wound dressings, systems applied over a wound to prevent complications and speed up recovery, is receiving increasing attention. Electrospun nanofibrous scaffolds gained great interest in the medical field due to their many advantages and beneficial characteristics. However, they are formed by of densely packed fiber layers, which render the available space between adjacent fibers minimal. In this study, nanometric fibers from pullulan polymeric blends were developed using cricket powder as novel component, due to its high chitin and chitosan content. Hydroxyapatite was also added due to its biocompatibility and capability to interact with the host tissues. The 2D mats based on electropsun fibers in membrane were converted to a 3D structure by gas foaming, involving $NaBH_4$. The obtained 3D systems were characterized for their morphology and composition, and mechanical properties. The scaffolds biocompatibility was tested on normal human dermal fibroblasts and mesenchymal stem cells, and cell adhesion was assessed. TNF-α secretion was thereafter characterized to evaluate the anti-inflammatory effects of the scaffolds on macrophages, and their antioxidant activity was also investigated. Finally, an evaluation of the scaffolds' safety and efficacy in vivo on a murine incisional and burn model was performed. The results obtained not only revealed greater structural and mechanical integrity of the gas-foamed scaffolds containing cricket powder, but also higher cytocompatibility towards different cell lines together with anti-inflammatory and antioxidant properties, thereby making them innovative tools to improve the process of wound healing.

1. Introduction

Skin plays a crucial role in various processes such as hydration and protection from chemicals and external microorganisms. Once its integrity is lost, skin is no longer a barrier, eventually letting microorganisms to invade and colonize the wound sites, which could result in a severe infection [1]. Wound healing is a well-regulated process composed by a complex series of overlapping events: hemostasis, inflammatory, proliferative and remodelling stages. However, chronic wounds, such as pressure ulcers, diabetic foot, and venous and arterial ulcers, do not reach structural and functional recovery, leading to an incomplete healing, which stalls in the inflammation phase [2,3].

If the organism is unable to achieve homeostasis after injury, a stop of the wound healing process occurs, resulting in impaired tissue regeneration. The inflammatory stage could persist longer than needed due to the excessive secretion of pro-inflammatory mediators causing delayed epithelialization and tissue necrosis [4]. Moreover, this could lead to microbial infections that could cause systemic disease, sepsis and ultimately death [5].

Globally, wound care is a major problem that poses big issues for national healthcare systems. Consequently, the development of wound dressings, systems applied over a wound to prevent complications and speed up recovery, is receiving increasing attention [6,7]. This highlights the needs of innovative tools of therapeutic intervention able to promote the process of wound healing.

In particular, polysaccharides have been suggested as biomaterials to improve the healing process due to their minimal toxicity, biocompatibility, and pharmacological biomedical activity, especially chitin,

* Corresponding author.
E-mail address: g.sandri@unipv.it (G. Sandri).
[1] These authors contributed equally to this work.

https://doi.org/10.1016/j.jddst.2024.105541
Received 19 January 2024; Received in revised form 1 March 2024; Accepted 5 March 2024
Available online 6 March 2024
1773-2247/© 2024 The Authors. Published by Elsevier B.V. This is an open access article under the CC BY-NC-ND license (http://creativecommons.org/licenses/by-nc-nd/4.0/).

chitosan, cellulose, and hyaluronan. Their antibacterial properties and capacity to lessen edema, inflammation, and wound exudate while promoting wound healing are of particular interest for the development of wound dressings [8].

Also, electrospun scaffolds gained great interest in the medical field due to their many advantages and beneficial characteristics. However, they are formed by of densely packed fiber layers, which render the available space between adjacent fibers minimal. This two-dimensional (2D) sheet-like structure with superficial planar pores is believed to restrict cell infiltration and growth into the scaffolds, which ultimately led to an increasing need of developing a new procedure capable of creating a threedimensional (3D) nanofibrous and porous structure that mimics the architecture of native extracellular matrix [9]. At this purpose, the gas foaming technique represents an innovative method to transform 2D nanofibrous systems in 3D structures. In particular, it is based on the nucleation and growth of gas bubbles in situ, which could be due to chemical reactions, or to the addition of inert gases to the polymer phase in different physical environments. It usually involves three basic steps: polymer/gas solution formation, gas bubbles (pore) nucleation and gas bubbles (pore) growth and volume expansion. Mahesh Kumar Joshi et al. describes a novel process of gas foaming using sodium borohydride ($NaBH_4$) solution, in which the electrospun scaffolds are incubated for different time intervals. The interconnected pores in the mat enhance the adsorption of the solution via capillary forces, followed by the hydrolysis of the solution yielding hydrogen (H_2) gas in situ. The H_2 gas molecules form clusters resulting in pore nucleation and causing an increase in the pores volume, creating a 3D architecture with loosely arranged fibers [9].

Given these premises, the present study aims at the design and the development of 3D gas foamed scaffolds. As novel component crickets were considered since they are a source of functional ingredients and bioactive compounds effective in tissue engineering such as essential amino acids (tryptophan, valine, histidine, isoleucine, leucine, lysine, methionine, phenylalanine, tyrosine, and threonine), and proteins; high concentration of vitamins including riboflavin, thiamine, folic acid, and niacin as well as a high concentration of minerals, especially iron, zinc, magnesium, calcium, salt, and potassium [10–12]. In fact, the entomotherapy is a traditional medicine that have been proven to effectively treat wounds as they are rich of bioactive compounds, including chitin, an insoluble fiber derived from the exoskeleton with great activity, such as antimicrobial, anti-inflammatory, antioxidant, and antifungicidal properties [13–16].

In these scaffolds hydroxyapatite (HP) nanoparticles doping has also been considered since it is widely used to treat and replace the damaged tissues. In fact, HP is described in literature as a bioactive compound characterized by good biocompatibility and degradability, which render it suitable for the interaction with the host tissues [17–19], being completely absorbed without causing any toxic effect in the host [17,20,21].

Whole frozen crickets were processed with acetic acid, then homogenized, and lastly combined with pullulan and HP. The scaffolds were prepared by means of electrospinning and then treated with $NaBH_4$ to obtain 3D structures by gas foaming. These were characterized by physico–chemical properties (morphology, dimensions, FTIR, and thermal analysis) and preclinical properties (fibroblast and mesenchymal stem cells adhesion and proliferation, anti-inflammatory and antioxidant properties, and efficiency in an in vivo wound incisional model) to assess their fate and effectiveness.

2. Materials and methods

2.1. Materials

Crickets (*Acheta domesticus*) (CR) were provided by Alia Insect Farm. Pullulan (PL), food grade (Hayashibara, Okayama, Japan) was used in order to optimize the electrospinning process, while citric acid (CA) (Carlo Erba Reagents, Cornaredo (MI), Italy) was involved as crosslinking agent. Hydroxyapatite (HP), nanopowder <200 nm particle size, 97% synthetic (Sigma-Aldrich, St. Louis, MO, USA) was used as inorganic component. Sodium borohydride ($NaBH_4$) (powder, ≥98.0%, MW: 37.83 g/mol) for the preparation of the gas foamed systems was purchased from Sigma-Aldrich (St. Louis, MO, USA).

2.2. Preparation of the polymeric blends

The crickets were harvested after 30 days of hatching and euthanized by rapid freezing in liquid nitrogen (as suggested by 2024 Guidelines for Protecting and Promoting Insect Welfare in Research, Insect Welfare Research Society). Then the whole crickets were dipped in water/acetic acid (1:1 vol ratio) in a concentration of 2% w/w. Later on, they were heated at 95 °C for 6 h. Thereafter, the obtained blend was mixed thoroughly by means of a rotor-stator homogenizer (IKA T25-Digital Ultra Turrax, Staufen, Germany) and filtered using stainless steel strainers with a 75 μm diameter (Endecotts Ltd., London, UK) as already described in a previous work [22]. The physico-chemical properties of the crickets (i.e. Fourier-transform infrared spectroscopy, thermal gravimetric analysis, and differential scanning calorimetry), their biological properties (i.e. chitin content, in vitro digestibility, antioxidant properties, and cytocompatibility and pro-inflammatory immune response) together to the stability and the standardization of the derived product are detailed in a previous work [15].

After the sieving process, PL (10% w/w) and CA (2% w/w) were added to the crickets dispersion. A similar blend was prepared with the addition of HP (2% w/w). A third blend, excluding the use of cricket, and containg PL (10% w/w), CA (2% w/w) and HP (2% w/w) was prepared in acetic acid (50% v/v in distilled water).

2.3. Preparation of the electrospun scaffolds

The scaffolds were manufactured using an electrospinning apparatus (STKIT-40, Linari Engineering, Pisa, Italy), high-voltage power supply (Razel R99-E 40 kV), and a volumetric pump (Razel R99-E) (voltage: 28 kV; flow: 0.595 cc/hr). A 10 mL syringe with inox 21G needle (inner diameter: 0.6 mm) was used. A flat static collector was used to obtain the scaffolds and the process was performed at atmospheric pressure, with the temperature and the relative humidity (RH) set in an established range of 25–35 °C and 25–35%, respectively. As a final step, the electrospun scaffolds were subjected to a crosslinking process using dry heating at 150 °C for 1 h [23]. This process is also reported as appropriate for sterilizing the products. In fact, dry heat seems to have the capability to penetrate and kill microorganisms via oxidation [24]. Moreover, the obtained systems were sterilized by steam (15 min at 121 °C) also resulted stable during steam sterilization in autoclave.

2.4. Gas foaming of the electrospun scaffolds

0.1 M $NaBH_4$ solution (Sigma Aldrich, Italy) was prepared in MilliQ water. The electrospun and crosslinked fibers were cut in 2 × 2 cm pieces and were then immersed in the $NaBH_4$ solution for 30 min at room temperature. The scaffolds were then washed with distilled water and vacuum dried for 5 min each, followed by freezing and then sublimation for 24 h in a Heto Drywinner sublimator (Analitica De Mori, Italia).

2.5. Physico-chemical characterization

The morphology of both electrospun fibers (before and after crosslinking process) and gas foamed systems was assessed by means of scanning electron microscopy (SEM; Tescan, Mira3XMU, Brno, Czech Republic). A sputtering with graphite under vacuum was used. The fibers dimensions and the pore area of the gas foamed systems were calculated using an image analysis software (ImageJ, ICY, Institut

Pasteur, Paris, France).

The scaffolds' composition was then characterized by SEM-Energy Dispersive X-ray Analysis (EDX), collecting the EDX spectra of the samples.

In order to investigate the swelling ratio (SR), the gas foamed scaffolds were weighted, immersed in water for 30 min, and then re-weighted. The following equation was used:

$$SR = \frac{W_S - W_D}{W_D} \times 100$$

where W_S represents the weight of the wet scaffolds, and W_D the initial weight of the dry scaffolds.

2.6. Structural characterization

Fourier-transform infrared (FT-IR) analysis was performed by means of a JASCO 6200 (Tokyo, Japan) equipped with a Ge ATR. The analyses were performed in a 400 to 4000 cm^{-1} wavenumber range, setting a resolution of 2 cm^{-1}. Afterwards, the results were processed using the Spectra Manager v2 software.

Thermogravimetric analyses (TGA) were performed by means of a STA (TG-DTA) equipment (Nexta200RV, Hitachi High-Tech America Inc., USA). The analyses were performed setting 25–1000 °C as temperature range with 10 °C/min heating rate, in atmospheric air (gas switch at 950 °C). Approximately 10 mg of sample were weighted in adequate sample holders.

2.7. Mechanical properties evaluation

Gas foamed scaffold systems were subjected to a compression test by means of a TA.XT plus apparatus (Stable Microsystems, Venezia, Italy), equipped with a measurement system A/TG (1 kg loading cell) and a spherical inox steel probe (Perspex probe, P/0.25S). All the analyses were conducted both in dry and hydrated state at room temperature.

2.8. DPPH radical scavenging assay

In order to assess the systems antioxidant capability, the scaffolds were weighed (around 10 mg) and placed at 37 °C in a phosphate-buffered saline solution (PBS, pH 7.4, Sigma-Aldrich, Milan, Italy). This allowed to simulate the scaffold implant in the lesion bed [25]. At prefixed times (0.5, 1, 2, and 8 h), the surpernatants were withdrawn to quantify the antioxidant properties of the samples by mixing each sample with a DPPH/methanol solution (8 μg/mL) in 1:1 vol ratio. After 30 min, DPPH radical scavenging activity was obtained by measuring absorbace (λ = 515 nm; FLUOstar® Omega, BMG LABTECH, Aylesbury, UK).

2.9. Cell adhesion and proliferation

Cytotoxicity and adhesion assays were carried out using two different cell types: fibroblasts (normal human dermal fibroblasts, NHDF, from juvenile foreskin, PromoCell, Milan, Italy) and hASCs cells (human adipose stem cells, ZenBio, Durham, NC, USA). The scaffolds were subjected to a steam sterilization process in autoclave and placed in a 24-well plate (flat bottom, Cellstar©, Greiner bio-one, Frickenhausen, Germany) and fibroblasts or hASCs were seeded onto the samples at 35 × 10^3 cells/well. After 3 or 6 days of growth, AlamarBlue (Thermo Fisher Scientific, Italy) assay was performed as already described in a previous work [26]. The fluorescence intensity (F.I.) was detected using a FLUOstar® Omega Microplate Reader at λex 560 nm and λem 590 nm.

Cells adhered onto the scaffolds were fixed using a glutaraldehyde solution (3% v/v in PBS) for 2 h at room temperature. FITC-phalloidin (green, Sigma-Aldrich, Milano, Italy; 50 μL/sample at 25 μg/mL in PBS) was used to stain cytoskeletons, and Hoechst 33258 (blue, Sigma-Aldrich, Milano, Italy; 50 μL/sample at 1:10,000 in PBS) was used to stain nuclei. Images were acquired using a Confocal Laser Scanning Microscope (CLSM, Leica TCS SP2, Leica Microsystems, Buccinasco (MI), Italy) with λex = 501 nm and λem = 523 nm for FITC-phalloidin, and λex = 346 nm and λem = 460 nm for Hoechst, and then processed with a software (Leica Microsystem, Buccinasco (MI), Italy).

2.10. Cytocompatibility of macrophages and pro-inflammatory immune response

Macrophages cytocompabitibility and pro-inflammatory immune response were carried out using hMoCD14 + -PB-c cell line (human $CD14^+$ monocytes derived from peripheral blood, Carlo Erba, Italy) as already described in a previous work [27]. An ELISA kit (Thermo Fisher, Italy) was used to evaluate the proinflammatory immune response by the quantification of the TNF-α (pro-inflammatory cytokine) secreted by macrophages. The method was linear (concentration range: 7.8–500 pg/mL; $R^2 > 0.995$). Lipopolysaccharide (LPS, 10 μg/mL for 24 h) was used as positive control [28].

2.11. In vivo evaluation

The animal experiments were compliant with the European Communities Council Directive 2010/63/EU. The protocol was approved by the University of Pavia and Istituto Superiore di Sanità (ISS). Eight male Wistar rats (Envigo RMS S.r.l.) with weights ranging from 200 g to 250 g were anesthetized with equitensine at 3 mL/kg. Their backs were then shaved to remove all hair as already described in previous works [25, 26].

2.11.1. Evaluation of systems safety

To evaluate the systems safety, an incision of 8 mm was made on the rat's back, allowing the subcutaneous implant of the gas foamed scaffolds; afterwards, the incisions were sutured. After 18 days, full thickness biopsies were taken in correspondence of the incisions and the histological analysis was performed as already described in a previous work [26]. Intact skin was taken for comparison, while treatment with NaCl 0.9% solution was considered as negative control.

After euthanasia, the skin portions corresponding to the incisions were immersed in the fixative solution (4% neutral buffered formaldehyde), then embedded in paraffin. Haematoxylin and eosin (H&E), and picrosirius red (PSR) were used for the samples staining. Stained sections were observed with a light microscope Carl Zeiss Axiophot provided for circular polarizing microscopy, with suitable filters in the condenser stage and in the microscope tube. Images were recorded through a microscope digital 5 megapixels CCD camera Nikon DS - Fi2.

2.11.2. Evaluation of systems efficacy

To evaluate the systems efficacy, an aluminium rod was used to produce three circular burns (diameter: 4 mm) on the rats' back (40 s of contact at 105 °C) as already described in a previous work by Ruggeri et al. [25].

Gas foamed scaffolds were applied into the lesions; treatment with NaCl 0.9% solution was considered as negative control. After 18 days, full thickness biopsies were taken in correspondence of the lesions and the histological analysis of the excised tissues was performed as described in Section 2.11.1. Intact skin was taken for comparison.

2.12. Statistical analysis

Statistical analyses were performed using Astatsa statistical calculator. 1-way ANOVA was followed by Scheffé post-hoc comparisons. $p < 0.05$ was considered significant.

3. Results

3.1. Physico-chemical characterization

Fig. 1a reports the pictures of the scaffolds before (left column) and after (right column) the gas foaming treatment, while Fig. 1b shows the SEM micrographs before (left column) and after (right column) the gas foaming treatment, and the SEM-EDX spectra (middle column).

The electrospun fibers are characterized by nanodimensions and rough surfaces, which should provide an increased cell anchorage to the surface (Fig. 1b, left column). Moreover, HP nanoparticles are clearly visible and embedded into the fibrous matrix of PL-HP and PL-CR-HP scaffolds and regular distribution into the matrix are confirmed by the EDX spectra (Fig. 1b, middle column). The 2D electrospun nanofibers are gradually modified into 3D structures upon treatment with $NaBH_4$ solution as observed in Fig. 1b (right column). In particular, the gas foamed scaffolds are characterized by pore areas of $175.79 \pm 31.70\ \mu m^2$, $79.63 \pm 28.89\ \mu m^2$, $29.12 \pm 7.91\ \mu m^2$ and swelling ratios of $87.17 \pm 14.80\%$, $77.91 \pm 8.45\%$, $81.17 \pm 14.20\%$ for PL-CR-HP, PL-HP, and PL-CR respectively. More importantly, the continuous and well-organized electrospun nanofibers are completely reorganized and macro-porosity together with 3D development occurs. The 3D organization of the scaffolds due to the microporosity suggests an increased suitability: the systems present a higher adaptability with a possible increase of the bioapplicability. The higher surface area of the scaffold and the increased porosity should facilitate cell migration and their homing. The foaming seems able to overcome the limitations posed by densely packed electrospun fibers that normally restrict cell growth and infiltration into the scaffold.

3.2. Structural characterization

Fig. 2a reports the FTIR profiles of the pure components (left), and of the gas foamed systems (right). The FTIR spectra of pristine CR shows the characteristic chitin peaks, in particular the one at around 3400 cm^{-1}, attributed to the $–NH_2$ and –OH groups stretching vibration, and the one at around 1630 cm^{-1}, corresponding to the C═O stretch of the amide I. Moreover, the spectra show pronounced IR absorption peaks at about 3000 cm^{-1} related to the CH_2 stretch of the lipids hydrocarbon chains [29]. Notably, HP PO_4^{3-} group forms intensive IR absorption bands at 560 cm^{-1} and 600 cm^{-1}, which are clearly visible also in the PL-HP and PL-CR-HP spectra, confirming the HP doping into the gas foamed structure [30]. This also confirms that HP is not dissolved during gas foaming process, remaining strictly embedded into the polymeric matrix.

Fig. 2b reports the TGA analyses of the scaffolds cross linked (CL), not cross linked (NCL), and gas foamed (GF), while Fig. 2c reports the TGA analyses of the pure components. As a general trend, all scaffolds

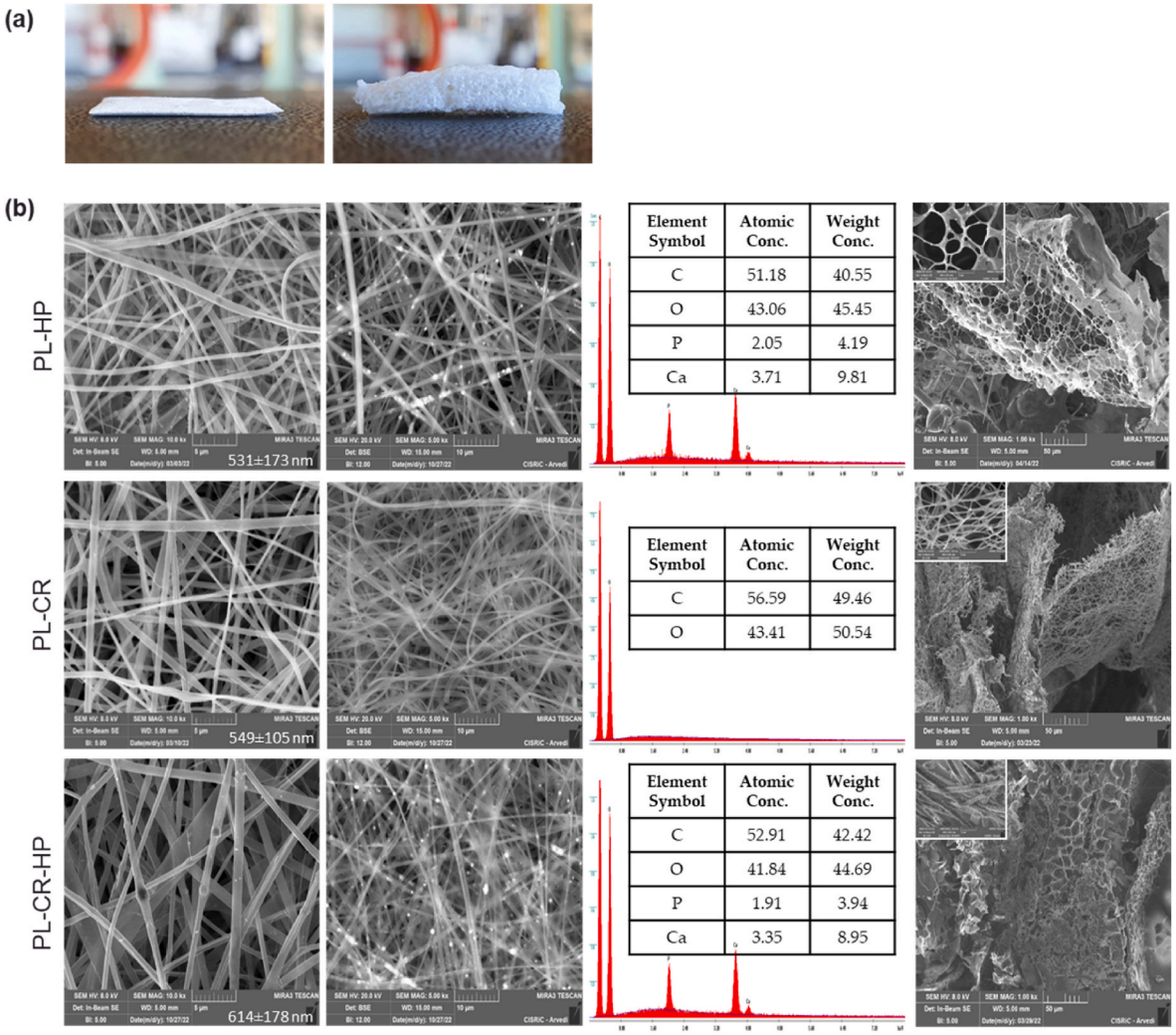

Fig. 1. (a) Pictures of the scaffolds before (left column) and after (right column) the gas foaming treatment; (b) SEM micrographs of the nanofibers before (left column), and after gas foaming (right column), and SEM-EDX spectra (middle column). In the insets, the corresponding dimensional analysis is reported (mean values ± s.d.; n = 90).

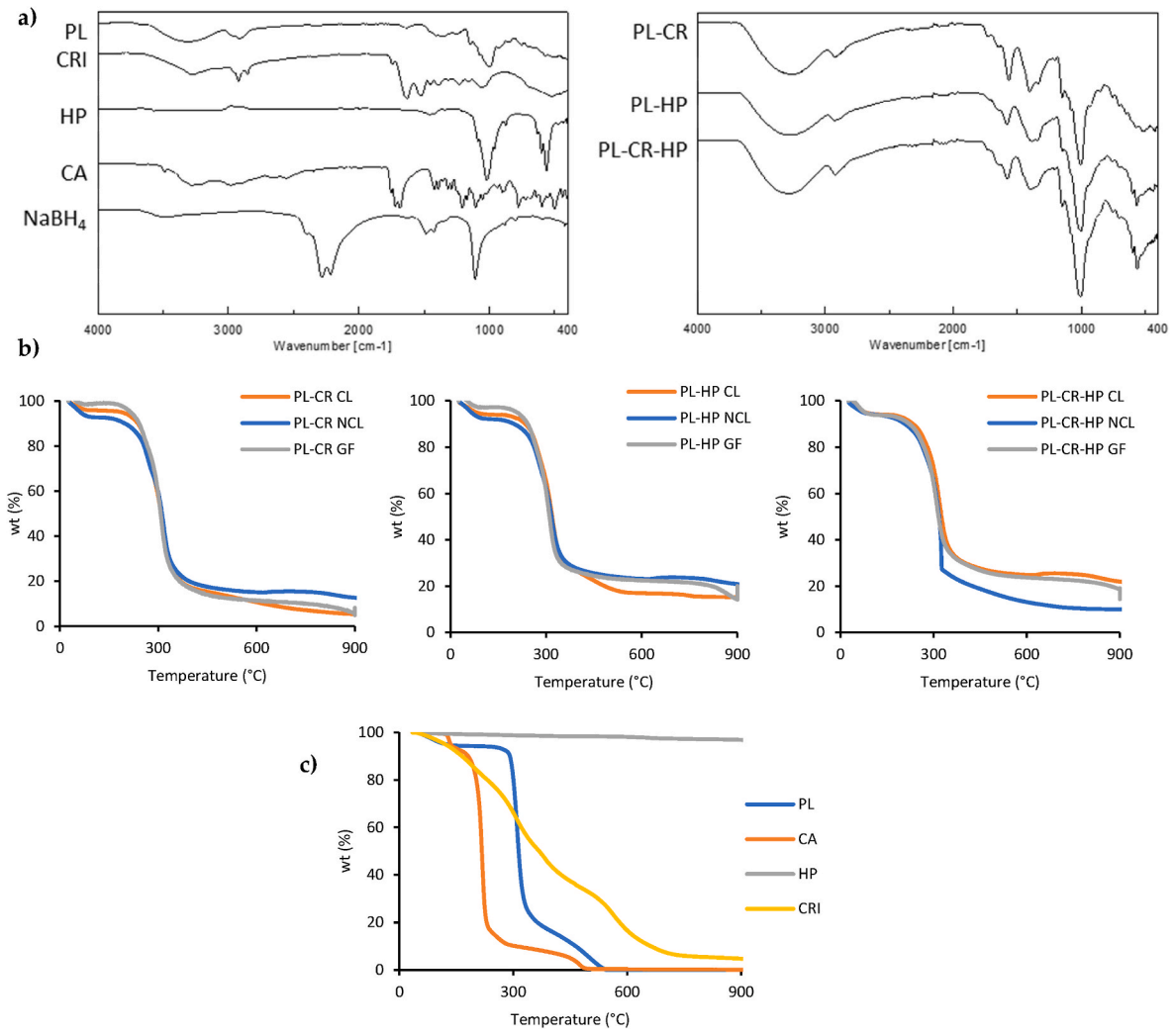

Fig. 2. (a) FTIR spectra of the pure components (left), and FTIR spectra of the gas foamed systems (right); (b) TGA analyses of the scaffolds cross linked (CL), not cross linked (NCL), and gas foamed (GF); (c) TGA analyses of the pure components.

show a weight loss in four stages. At first, the CL and GF scaffolds are characterized by a 4% weight loss at around 92 °C, while the NCL are characterized by an initial weight loss of about 7%. This is followed by a plateau in the 94–240 °C temperature range, suggesting a thermal stability, and then by an intense weight loss in the 250–360 °C temperature range, that is conceivably related to degradation. This ends at about 580 °C. The scaffolds show similar thermograms and final residues of around 5% for the PL-CR scaffolds, and 20% and 18% for PL-HP and PL-CR-HP scaffolds respectively. This seems related to HP residues, as reported by Lim et al. [12,31]. Moreover, the thermal analysis also

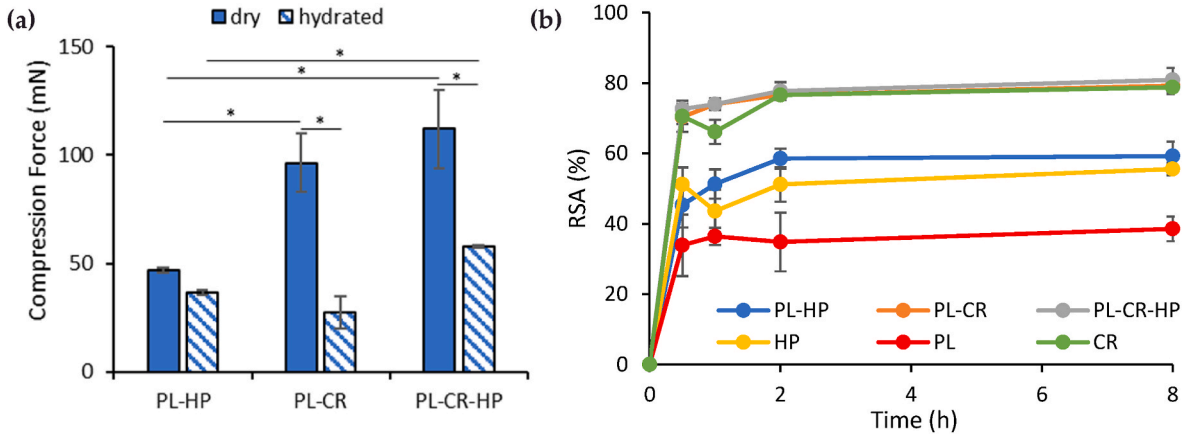

Fig. 3. (a) Force of compression of PL-HP, PL-CR, and PL-CR-HP gas foamed scaffolds (mean values ± s.d.; n = 4); (b) DPPH scavenging activity of the scaffolds (mean values ± s.d.; n = 6). * indicates statistical differences between results.

confirmed that no significant residues of $NaBH_4$ or the reaction product ($NaBO_2$) remained into the matrices. This is supported by the reaction of hydrogen generation that is quantitative, giving H_2 as gaseous product. Moreover, the $NaBO_2$ should be washed away after the reaction. Eventual traces of $NaBO_2$ (melting point at 60 °C with decomposition) should decompose during the thermal treatment (stem sterilization) since no B related signals are visible in FTIR spectrum. In fact, TGA spectra of the GF scaffolds result almost superimposable to the ones of the CL and NCL fibers, suggesting no further weight loss attributable to B related compounds [32].

3.3. Mechanical properties evaluation

Fig. 3a reports the mechanical properties of the gas foamed scaffolds. The force of compression in the hydrated state shows an overall decrease for all the scaffolds when compared to the ones in dry state. This could easily be related to the level of hydration of the systems, that could compromise their integrity. Notably, the crickets have an advantageous impact on mechanical properties of the gas foamed systems, as the compression forces of PL-CR and PL-CR-HP systems are significantly higher than that of PL-HP. In particular, the combination of crickets and HP resulted in the highest mechanical properties, both in dry and hydrated state. This should be due to the dispersion of the HP nanoparticles and the crickets that increase the system resistance to the compression. In fact, chitin, a key component of crickets, is a not soluble polymer in aqueous environment, and, although the mechanical resistance to the compression is retained upon hydration, the system is much more plastic. The synergism between the HP nanoparticles and the chitin from crickets allows to maintain the better mechanical properties also in hydrated state.

3.4. DPPH radical scavenging assay

A scaffold having antioxidant properties could constitute an interesting tool to balance the radical oxygen species (ROS) during the inflammation phase of the healing process. In fact, ROS have a positive effect on angiogenesis and reepithelization, protecting the site from infections, but they could also lead to a negative effect when present at high concentration, impairing cell proliferation and migration. The antioxidant activity is fundamental to inhibit the formation of free radicals and prevent the damage that could be caused to the cells. For this reason, antioxidant properties of the gas foamed scaffolds were characterized by DPPH assay, evaluating their capability to reduce the stable radical DPPH. Fig. 3b reports the antioxidant properties of the scaffolds and of the pure components (CR, HP, and PL) reported as radical scavenging activity (RSA%). It is possible to observe that the scaffolds with CR are characterized by a higher RSA % than the scaffolds PL-HP. This antioxidant activity is mainly due to the free radical-scavenging activities of the chitin contained in CR. In fact, chitin is able to promote a positive impact on several biological functions, acting as antioxidant compounds [33]. In particular, chitin antioxidant activity is related to the presence of protonated amide groups together with the ability to chelate metal ions that induce formation of free radicals in cells [34].

Moreover, all scaffolds are characterized by RSA% which reaches a plateau after 1 h, suggesting the complete release of bioactive molecules.

3.5. Cell adhesion and proliferation

Fig. 4a reports cytotoxicity results towards NHDF grown onto the gas foamed scaffolds after 3 and 6 days of culture, while Fig. 4b reports the alamar blue assay performed on hASCs grown onto the gas foamed scaffolds after 3 and 6 days of culture. Both cell lines are able to grow onto the scaffolds with a cell growth superimposable to that of the positive control (GM). In particular, the combination of CR and HP seems to effectively enhance the hASCs proliferation, which is higher than that of the positive control (GM). Moreover, all substrates result optimal for the cell adhesion, as shown in Fig. 4c. In fact, both NHDF (Fig. 4c, upper line) and hASCs (Fig. 4c, lower row) are able to adhere and colonize the gas foamed scaffolds after 6 days of culture.

3.6. Cytocompatibility of macrophages and pro-inflammatory immune response

The TNF-α release, related to the anti-inflammatory properties of the gas foamed scaffolds, was evaluated by means of an ELISA assay. Macrophages were put in contact with lipopolysaccharide (LPS) to cause an inflammatory reaction, then the scaffolds extracts were put in contact with the cells.

Fig. 4d reports the macrophages viability in terms of optical density (O.D.) after the contact with the scaffolds' extracts, while Fig. 4e reports the concentration values of the TNF-α secreted by the macrophages after the contact with the scaffolds' extracts. It is possible to observe that the extracts do not contain any toxic component, resulting cytocompatible with a cell viability similar to the positive control (GM and LPS). Moreover, all the scaffolds, and especially the ones composed by CR, lead to a decrease of the TNF-α secretion in 24 h, reaching values significantly lower than that of the LPS. This suggests that the scaffolds are able to decrease the inflammatory response over time.

3.7. In vivo evaluation

Fig. 5 shows the images of the systems safety evaluation. Skin sections of the subcutaneous implant, stained with haematoxylin and eosin (H&E) (left panel), and Picrosirius red (PSR) (central panel: with bright-field images; right panel: with polarized light), are reported. The lesions treated with saline solution (Fig. 5b) show an area covered by the eschar (red arrows) and not fully re-epithelialized. A large amount of granulation tissue is visible, with extensive neoangiogenesis (black arrow) and a large area of about 5 mm of immature and not-remodelled collagen (white arrows), both type III (green fibers) and type I (red fibers). On the other hand, completely regenerated epithelium is assessable in every lesion treated with the gas foamed scaffolds. In particular, in subcutaneous implant of PL-CR-HP (Fig. 5e) the wound area is hardly recognizable from the adjacent control skin and collagen fibers are also remodelled in an orderly pattern. It shows an epidermal layer fully restored in multiple layers of cells and with a fair degree of keratinization. Skin appendages such as hair follicles and glands are identical in number and disposition to those of intact skin. Subcutaneous PL-HP (Fig. 5c) shows well-formed keratinized squamous epithelium with normal collagen (white arrows; collagen type III: green fibers, collagen type I: red fibers) in the underlying dermis. Only a few tens of microns area in remodelling and the formation of skin annexes are visible. PL-CR implant (Fig. 5d) is the less healed. A small area not yet re-epithelized and covered by eschar (red arrow), with granulation tissue and neoangiogenesis (blak arrow), is visible, together with a small area with newly formed and not yet organized collagen (white arow). However, all subcutaneous implants of the gas foamed scaffolds do not cause any inflammatory effect, with no leukocyte recruitment or foreign body response, ulteriorly confirming that also no significant residues of $NaBH_4$ are present into the matrices.

Fig. 6 shows the images of the systems efficacy evaluation. Wound area sections stained with haematoxylin and eosin (H&E) (left panel), and Picrosirius red (PSR) (central panel: with bright-field images; right panel: with polarized light), are reported. In the lesions treated with PL-CR-HP (Fig. 6e) the wound area is covered by a thin epithelium and by eschar (red arrow). Granulation tissue and neoangiogenesis (black arrows) are also observed, with newly formed collagen not yet organized (white arrows; collagen type III (green fibers) not already replaced by collagen type I). The lesion treated with PL-HP (Fig. 6c) is completely re-epithelized, showing a small area of about 800 μm of granulation tissue and neoangiogenesis (black arrows). In the same area, newly formed

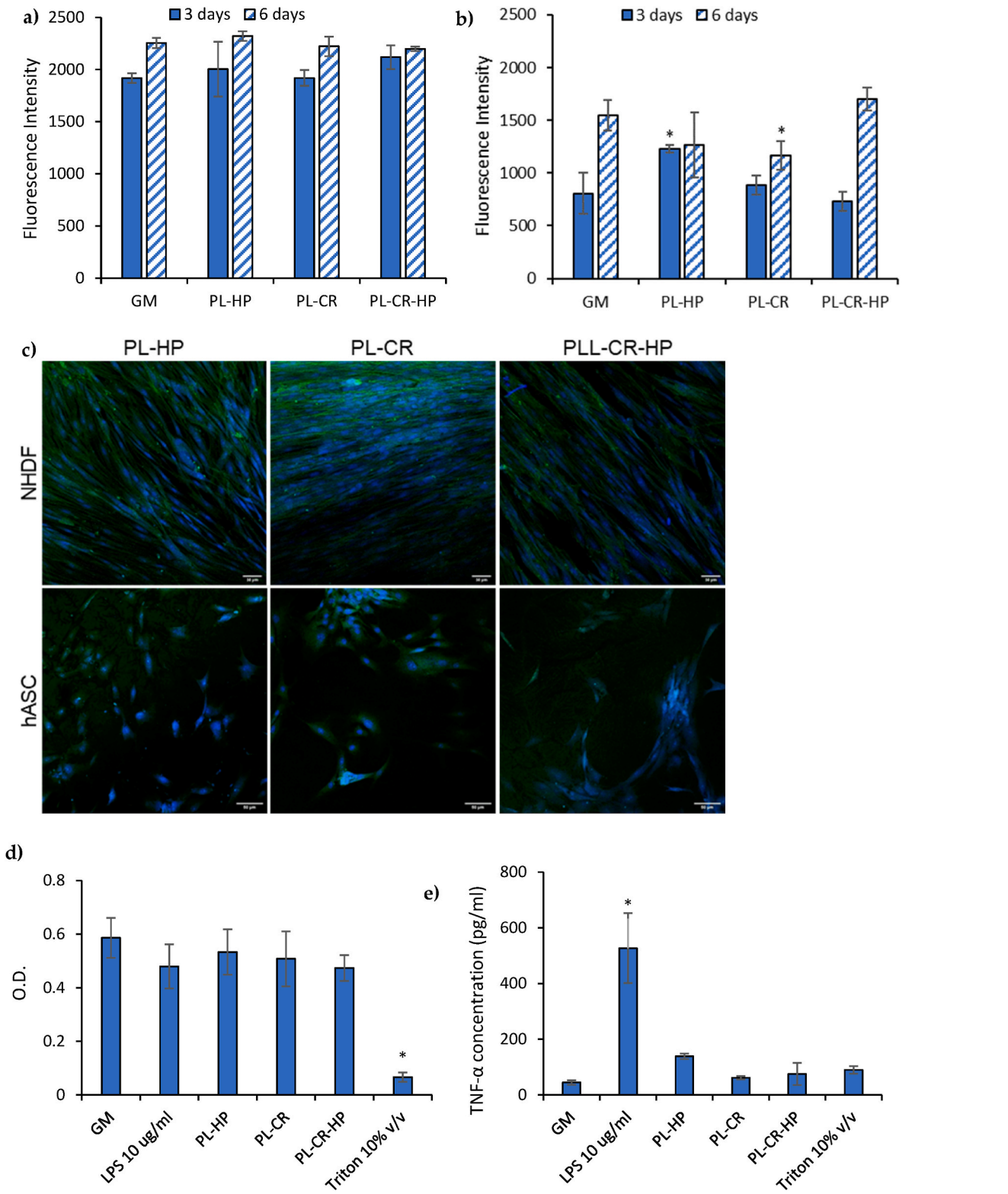

Fig. 4. (a) Alamar blue assay performed on NHDF grown onto the PL-CR, PL-HP and PL-CR-HP scaffolds after 3 and 6 days of culture; (b) Alamar blue assay performed on hASCs grown onto the PL-CR, PL-HP and PL-CR-HP scaffolds after 3 and 6 days of culture (GM: positive control); (c) CLSM images of NHDF and hASCs cells grown onto PL-CR, PL-HP and PL-CR-HP gas foamed scaffolds at 6 days of culture (nuclei stained in blue, cytoskeleton stained in green; scale bar 50 μm); (d) cytocompatibility of macrophages (O.D.- optical density) of the scaffolds after 24 h of contact; (e) secreted TNF-α concentrations (pg/ml) after cells exposure to scaffolds (GM: growth medium; LPS: lipopolysaccharide) (mean values ± s.d.; n = 8). * indicates statistical differences with the positive control GM. (For interpretation of the references to colour in this figure legend, the reader is referred to the Web version of this article.)

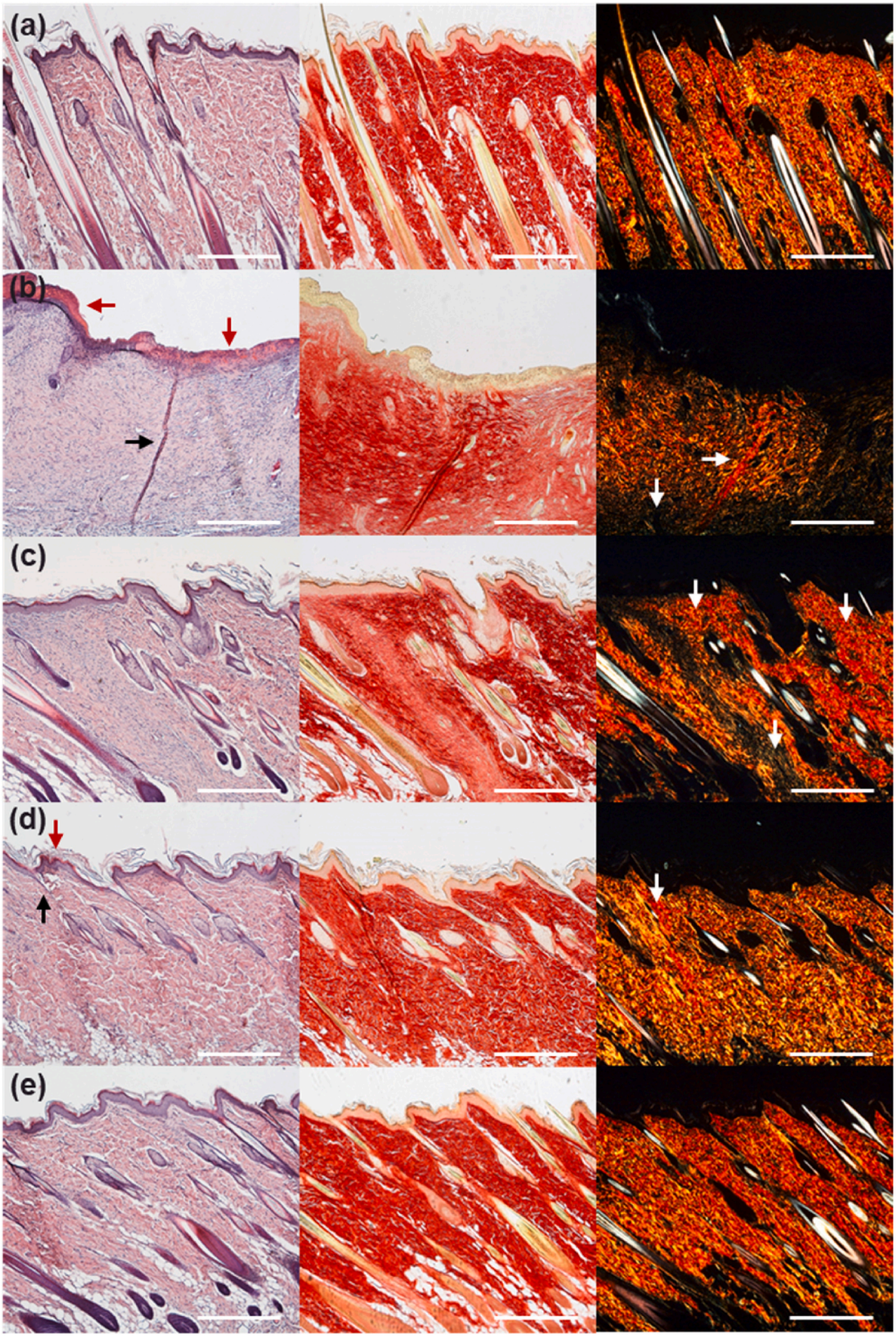

Fig. 5. In vivo safety evaluation of the scaffolds: H&E (left panel) and PSR sections (central panel: bright-field images; right panel: polarized light images) of (a) intact skin, (b) lesion treated with NaCl 0.9% solution (negative control), (c) subcutaneous implant of PL-HP scaffold, (d) subcutaneous implant of PL-CR scaffold, (e) subcutaneous implant of PL-CR-HP scaffold (black arrows: neoangiogenesis; red arrows: eschar; white arrows: collagen). Original magnification: 5 × , frame width: 1780 μm (scale bar: 500 μm). (For interpretation of the references to colour in this figure legend, the reader is referred to the Web version of this article.)

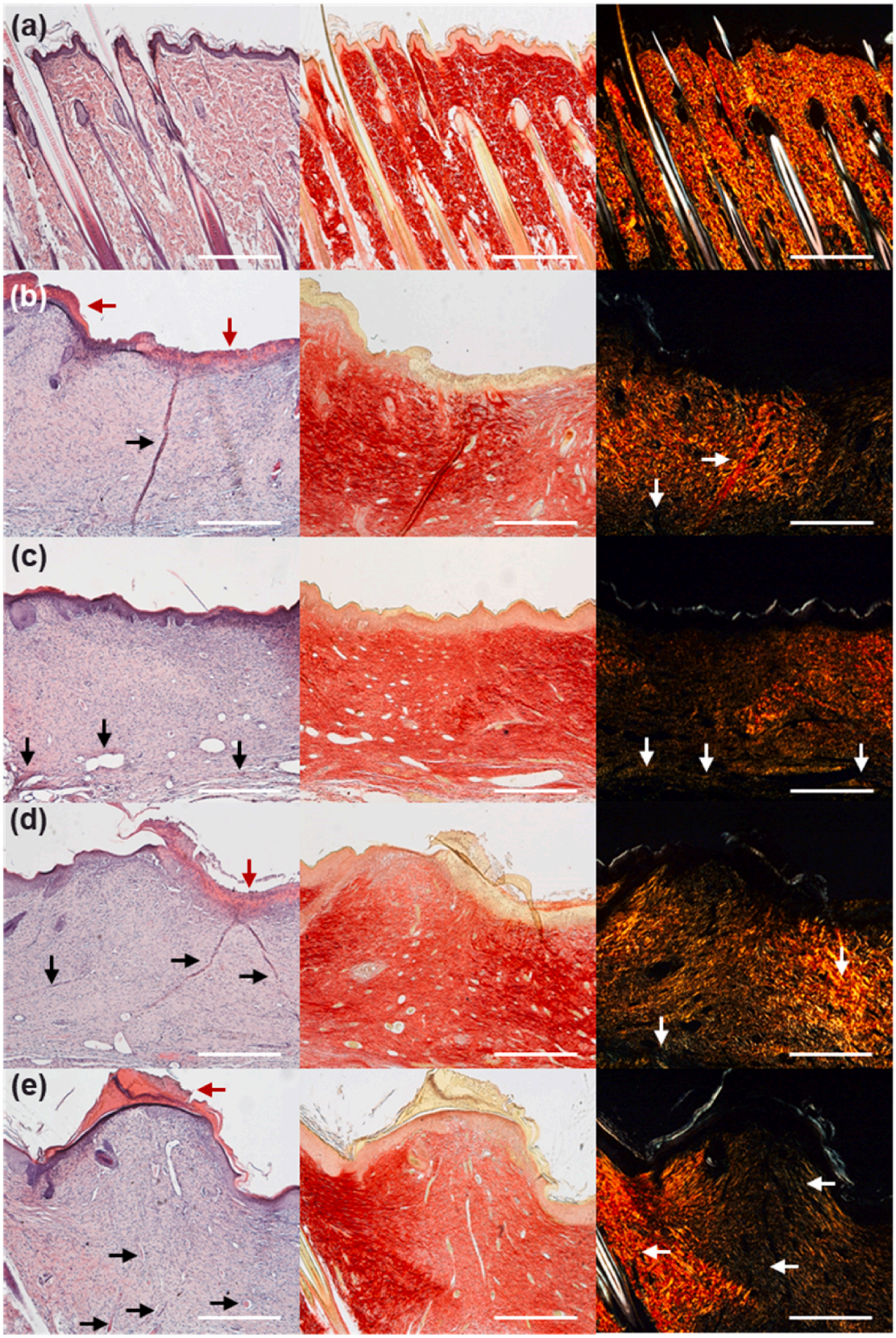

Fig. 6. In vivo efficacy evaluation of the scaffolds: H&E (left panel) and PSR sections (central panel: bright-field images; right panel: polarized light images) of (a) intact skin, (b) lesion treated with NaCl 0.9% solution (negative control), (c) lesion treated with PL-HP scaffold, (d) lesion treated with PL-CR scaffold, (e) lesion treated with PL-CR-HP scaffold (black arrows: neoangiogenesis; red arrows: eschar; white arrows: collagen). Original magnification: 5 × , frame width: 1780 μm (scale bar: 500 μm). (For interpretation of the references to colour in this figure legend, the reader is referred to the Web version of this article.)

collagen (white arrows; collagen type III: green fibers, collagen type I: red fibers) is found in remodelling. As regards PL-CR treated lesion (Fig. 6d), the healing results similar to the safety evaluation, showing a small area of granulation tissue and neoangiogenesis (black arrows) and covered by eschar (red arrow), together with a small area with newly formed and not yet organized collagen (white arrows; collagen type III: green fibers, collagen type I: red fibers). However, all lesions treated with gas foamed scaffolds were able to heal better than the control treated with saline solution. Moreover, no sign of scaffolds residuals is visible in the wound area, meaning that the systems are able to achieve a complete degradation in vivo during the 18 days of treatment.

4. Conclusions

Nanofibrous scaffolds based on PL and CR and doped with HP were manufactured using the electrospinning technique and converted in 3D systems using the gas foaming technique.

The presence of CR and HP leads to the formation of rougher fibers, which is desirable to provide an increased cell anchorage to the surface. SEM-EDX confirms the encapsulation of HP into the matrix and its regular distribution into the scaffolds. The presence of CR increases the scaffolds mechanical properties both in dry and hydrated state, and in particular, the combination of CR and HP results in the highest mechanical properties. PL-CR and PL-CR-HP scaffolds are characterized by remarkable antioxidant properties, as they are characterized by an RSA % of about 80% after 2 h, representing an important tool to balance the ROS during the inflammation phase of the healing process.

The scaffolds result biocompatible towards NHDF and hASCs, and they are able to support cell adhesion and proliferation in vitro after 6 days of culture. They also result cytocompatible towards macrophages, showing a cell viability similar to the positive control, meaning that the scaffolds do not release any cytotoxic component. Moreover, all the scaffolds, and in particular the ones with CR, lead to a decrease of the TNF-α secretion in 24 h, suggesting that the scaffolds decrease the inflammatory response over time.

Finally, the gas foamed scaffolds implanted in vivo on a murine model lead to a greater regeneration of the lesion than the control treated with saline solution. Moreover, the systems result safe, as they do not cause any inflammatory effect, with no leukocyte recruitment or foreign body response.

In conclusion, gas foamed nanofibers based on CR and doped with HP seem to be promising in mimicking the native extracellular matrix and restoring the skin tissue. This novel study, critically detailing the advantages of using CR in the development of biopolymeric scaffolds aimed at improving the process of wound healing, is therefore of very high therapeutic potential.

Funding

This research did not receive any specific grant from funding agencies in the public, commercial, or not-for-profit sectors.

CRediT authorship contribution statement

Eleonora Bianchi: Writing – review & editing, Writing – original draft, Validation, Software, Methodology, Investigation, Formal analysis, Data curation, Conceptualization. **Marco Ruggeri:** Writing – review & editing, Writing – original draft, Validation, Software, Methodology, Investigation, Formal analysis, Data curation, Conceptualization. **Barbara Vigani:** Visualization, Validation. **Carlotta Totaro Fila:** Resources. **Antonia Icaro Cornaglia:** Investigation. **Cinzia Boselli:** Investigation. **César Viseras:** Resources, Investigation. **Silvia Rossi:** Visualization, Supervision, Resources, Funding acquisition. **Giuseppina Sandri:** Writing – review & editing, Writing – original draft, Supervision, Resources, Project administration, Methodology, Funding acquisition, Conceptualization.

Declaration of competing interest

The authors declare that they have no known competing financial interests or personal relationships that could have appeared to influence the work reported in this paper.

Data availability

Data will be made available on request.

Acknowledgments

This work is part of the project NODES which has received funding from the MUR - M4C2 1.5 of PNRR funded by the European Union - NextGenerationEU (Grant agreement no. ECS00000036).

References

[1] M. Ruggeri, B. Vigani, C. Boselli, A. Icaro Cornaglia, D. Colombo, R. Sanchez-Espejo, E. Del Favero, N. Mandras, J. Roana, L. Cavallo, L. Cantù, C. Viseras, S. Rossi, G. Sandri, Smart nano-in-microparticles to tackle bacterial infections in skin tissue engineering, Mater. Today Bio 16 (2022) 100418, https://doi.org/10.1016/j.mtbio.2022.100418.

[2] I. De Luca, P. Pedram, A. Moeini, P. Cerruti, G. Peluso, A. Di Salle, N. Germann, Nanotechnology development for for-mulating essential oils in wound dressing materials to promote the wound-healing process: a review, Appl. Sci. 11 (2021) 1713, https://doi.org/10.3390/app11041713.

[3] M. Ruggeri, E. Bianchi, S. Rossi, B. Vigani, M.C. Bonferoni, C. Caramella, G. Sandri, F. Ferrari, Nanotechnology-based medical devices for the treatment of chronic skin lesions: from research to the clinic, Pharmaceutics 12 (2020), https://doi.org/10.3390/pharmaceutics12090815.

[4] A. Toma, J. Fuller, N. Willett, S. Goudy, Oral wound healing models and emerging regenerative therapies, Transl. Res. 236 (2021) 17–34, https://doi.org/10.1016/j.trsl.2021.06.003.

[5] K.B. Thompson, L.T. Krispinsky, R.J. Stark, Late immune consequences of combat trauma: a review of trauma-related immune dysfunction and potential therapies, Military Med. Res. 6 11 (2019), https://doi.org/10.1186/s40779-019-0202-0.

[6] R. Dong, B. Guo, Smart wound dressings for wound healing, Nano Today 41 (2021) 101290, https://doi.org/10.1016/j.nantod.2021.101290.

[7] H. Derakhshandeh, S.S. Kashaf, F. Aghabaglou, I.O. Ghanavati, A. Tamayol, Smart bandages: the future of wound care, Trends Biotechnol. 36 (2018) 1259–1274, https://doi.org/10.1016/j.tibtech.2018.07.007.

[8] Y. Yang, L. Xu, J. Wang, O. Meng, S. Zhong, Y. Gao, X. Cui, Recent advances in polysaccharide-based self-healing hydrogels for biomedical applications, Carbohyd. Polym. 283 (2022) 119161, https://doi.org/10.1016/j.carbpol.2022.119161.

[9] M. Joshi, H. Pant, A. Tiwari, H. Kim, C. Park, C. Kim, Multi-layered macroporous threedimensional nanofibrous scaffold via a novel gas foaming technique, J. Chem. Eng. 275 (2015) 79–88, https://doi.org/10.1016/j.cej.2015.03.121.

[10] K. Ganguly, S.D. Dutta, M.S. Jeong, D.K. Patel, S.J. Cho, K.T. Lim, Naturally derived protein extract from Gryllus bimac-ulatus improves antioxidant properties and promotes osteogenic differentiation of hBMSCs, PLoS One 16 (2021) e0249291, https://doi.org/10.1371/journal.pone.0249291.

[11] D.K. Murugu, A.N. Onyango, A.K. Ndiritu, I.M. Osuga, C. Xavier, D. Nakimbugwe, C.M. Tanga, From farm to fork: crickets as alternative source of protein, minerals, and vitamins, Front. Nutr. 8 (2021) 704002, https://doi.org/10.3389/fnut.2021.704002.

[12] H.J.O. Magara, S. Niassy, M.A. Ayieko, M. Mukundamago, J.P. Egonyu, C. M. Tanga, E.K. Kimathi, J.O. Ongere, K.K.M. Fiaboe, S. Hugel, M.A. Orinda, N. Roos, S. Ekesi, Edible crickets (orthoptera) around the World: distribution, nutritional value, and other benefits-A review, Front. Nutr. 7 (2021) 537915, https://doi.org/10.3389/fnut.2020.537915.

[13] M.M. Zimmer, J. Frank, J.H. Barker, H. Becker, Effect of extracts from the Chinese and European mole cricket on wound epithelialization and neovascularization: in vivo studies in the hairless mouse ear wound model, Wound Repair Regen. 14 (2006) 142–151, https://doi.org/10.1111/j.1743-6109.2006.00104.x.

[14] L. Mozhui, L.N. Kakati, V.B. Meyer-Rochow, Entomotherapy: a study of medicinal insects of seven ethnic groups in Nagaland, North-East India, J. Ethnobiol. Ethnomed. 17 (2021) 17, https://doi.org/10.1186/s13002-021-00444-1.

[15] M. Ruggeri, E. Bianchi, B. Vigani, R. Sànchez-Espejo, M. Spano, C. Totaro Fila, L. Mannina, C. Viseras, S. Rossi, G. Sandri, Nutritional and functional properties of novel Italian spray-dried cricket powder, Antioxidants 12 (2023) 112, https://doi.org/10.3390/antiox12010112.

[16] A. Jantzen da Silva Lucas, E. Quadro Oreste, N. Leão Gouveia Costa, H. Martín Lòpez, H. Dias Medeiros Saad, C. Prentice, Extraction, physicochemical characterization, and morphological properties of chitin and chitosan from cuticles of edible in-sects, Food Chem. 343 (2021) 128550, https://doi.org/10.1016/j.foodchem.2020.128550.

[17] E. Bianchi, B. Vigani, C. Viseras, F. Ferrari, S. Rossi, G. Sandri, Inorganic Nanomaterials in tissue engineering, Pharmaceutics 14 (2022) 1127, https://doi.org/10.3390/pharmaceutics14061127.

[18] P. Kumar, B.S. Dehiya, A. Sindhu, Bioceramics for hard tissue engineering applications: a review, Int. J. Appl. Eng. Res. 13 (2018) 2744–2752, https://doi.org/10.3844/ajbbsp.2006.49.56.
[19] A. Faccendini, E. Bianchi, M. Ruggeri, B. Vigani, C. Perotti, F.C. Pavesi, L. Caliogna, F. Natali, E. Del Favero, L. Cantu, F. Ferrari, S. Rossi, G. Sandri, Smart device for biologically enhanced functional regeneration of osteo–tendon interface, Pharmaceutics 13 (2021) 1996, https://doi.org/10.3390/pharmaceutics13121996.
[20] M. Fathi-Achachelouei, H. Knopf-Marques, C.E. Ribeiro da Silva, J. Barthès, E. Bat, A. Tezcaner, N.E. Vrana, Use of na-noparticles in tissue engineering and regenerative medicine, Front. Bioeng. Biotechnol. 7 (2019) 113, https://doi.org/10.3389/fbioe.2019.00113.
[21] C. Yao, J. Zhu, A. Xie, Y. Shen, H. Li, B. Zheng, Y. Wei, Graphene oxide and creatine phosphate disodium dual tem-plate-directed synthesis of GO/hydroxyapatite and its application in drug delivery, Mater. Sci. Eng. C 73 (2017) 709–715, https://doi.org/10.1016/j.msec.2016.11.083.
[22] M. Ruggeri, B. Vigani, E. Bianchi, C. Valentino, C. Totaro Fila, C. Boselli, A. Icaro Cornaglia, C. Viseras, S. Rossi, G. Sandri, Hydroxyapatite-doped microspheres in chronic wound regeneration, J. Drug Deliv. Sci. Technol. 86 (2023) 104758, https://doi.org/10.1016/j.jddst.2023.104758.
[23] T.C. Kupiec, P. Matthews, R. Ahmad, Dry-heat sterilization of parenteral oil vehicles, Int. J. Pharm. Compd. 4 (2000) 223–224.
[24] S.E. Walsh, K. Laird, J.Y. Maillard, Principles of sterilization, in: K.M.G. Taylor (Ed.), Aulton's Pharmaceutics: the Design and Manufacture of Medicines, M.E. Aulton, 2022.
[25] M. Ruggeri, E. Bianchi, S. Rossi, C. Boselli, A. Icaro Cornaglia, L. Malavasi, R. Carzino, G. Suarato, R. Sánchez-Espejo, A. Athanassiou, C. Viseras, F. Ferrari, G. Sandri, Maltodextrin-amino acids electrospun scaffolds cross-linked with Maillard-type reaction for skin tissue engineering, Biomater. Adv. 133 (2022) 112593, https://doi.org/10.1016/j.msec.2021.112593.
[26] E. Bianchi, M. Ruggeri, B. Vigani, E. Del Favero, C. Ricci, C. Boselli, A. Icaro Cornaglia, A. Viseras, S. Rossi, G. Sandri, Cerium oxide and chondroitin sulfate doped polyurethane scaffold to bridge tendons, ACS Appl. Mater. Interfaces 15 (22) (2023) 26510–26524, https://doi.org/10.1021/acsami.3c06144.
[27] E. Bianchi, B. Vigani, M. Ruggeri, E. Del Favero, C. Ricci, P. Grisoli, A. Ferraretto, S. Rossi, C. Viseras, G. Sandri, Elec-trospun scaffolds based on poly(butyl cyanoacrylate) for tendon tissue engineering, Int. J. Mol. Sci. 24 (2023) 3172, https://doi.org/10.3390/ijms24043172.
[28] Y.Y. Lim, T.T. Lim, J.J. Tee, Antioxidant properties of several tropical fruits: a comparative study, Food Chem. 103 (2007) 1003–1008.
[29] D. El montassir, T. Moha, N. Eladlani, M. Rhazi, Extraction and characterization of chitin and chitosan from parapenaeus longirostris from Moroccan local sources, Int. J. Polym. Anal. 19 (2015) 342–351, https://doi.org/10.1080/1023666X.2014.902577.
[30] H. Gheisari, E. Karamian, M. Abdellahi, A novel hydroxyapatite –Hardystonite nanocomposite ceramic, Ceram. Int. 41 (2015) 5967–5975, https://doi.org/10.1016/j.ceramint.2015.01.033.
[31] S.J. Lim, W.M. Wan Aida, M.Y. Maskat, J. Latip, K.H. Badri, O. Hassan, B. M. Yamin, Characterisation of fucoidan extracted from Malaysian Sargassum binderi, Food Chem. 209 (2016) 267–273, https://doi.org/10.1016/j.foodchem.2016.04.058.
[32] C.J. Tomasso, A.L. Pham, T.M. Mattox, J.J. Urban, Using additives to control the decomposition temperature of sodium borohydride, J. Energy Power Supply 2 (2020), https://doi.org/10.21926/jept.2002009.
[33] F.M. de Matos, P. Kern Novelli, R.J. Soares de Castro, Enzymatic hydrolysis of black cricket (Gryllus assimilis) proteins posi-tively affects their antioxidant properties, J. Food Sci. 86 (2021) 571–578, https://doi.org/10.1111/1750-3841.15576.
[34] V.P. Varlamov, A.V. Il'ina, B.Ts Shagdarova, A.P. Lunkov, I.S. Mysyakina, Chitin/chitosan and its derivatives: funda-mental problems and practical approaches, Biochemistry (Mosc.) 85 (2020) 154–176, https://doi.org/10.1134/S000629792014008.